

Use of SiO₂ - TiO₂ Nanocomposite as Photocatalyst for the Removal of Trichlorophenol: A Kinetic Study and Numerical Evaluation

Heba Gobara*, Radwa El-Salamony, Dalia Mohamed, Marwa Mishrif, Yasser Moustafa and Tahani Gendy

Egyptian petroleum Research Institute, PO box 11727, Cairo, Egypt

* E-mail of the corresponding author: hebagobara@gmail.com

Abstract

A series of silica-titania nanocomposite materials with different silica–titania ratios was prepared in presence of a novel ethoxylated sulphanilamide of molecular weight 1053 by the sol-gel method. Several characterisation techniques were adopted such as thermal analysis (differential scanning calorimetry (DSC) and thermal gravimetric analysis (TGA)), N₂-adsorption-desorption, X-ray diffraction (XRD), Fourier transform infrared (FTIR), and transmission electron microscopy (TEM) connected with energy dispersive spectroscopy (EDS). The surface acidity was investigated by pyridine adsorption using FTIR spectroscopy. The photocatalytic activity and the adsorptive ability of the composites were evaluated based on the photodegradation of 2, 4, 6-trichlorophenol (TCP) under UV irradiation with a wavelength of 254 nm. The maximum TCP adsorption onto the composites was measured in darkness. The results showed that there was no adsorption of TCP on pure SiO₂. The 10% TiO₂-SiO₂ catalyst showed the highest rate of TCP removal among the synthesised composites. The removal % reached to 87 % after 90 min irradiation time. This activity was caused by the large surface area and pore volume as well as the formation of a mesoporous structure, as evidenced from the pore size distribution curve. Finally, the numerical evaluation of the photodegradation of TCP was conducted.

Keywords: Nanocomposite, Ethoxylated sulphanilamide, Photocatalytic degradation, UV irradiation, 2,4,6-TCP, Numerical evaluation.

1. Introduction

The importance of titania photocatalysis in environmental improvement such as the photodegradation and complete mineralisation of organic pollutants, has continuously increased (**Linsebigler et al. 1995; Fujishima et al. 2000**). TiO₂ nanoparticles have high catalytic performance and large specific surface areas in which reactions take place. However, their effective commercial applications are hindered by two serious disadvantages. First, the agglomeration of ultrafine powders into larger particles, resulting in an adverse effect on the catalyst performance. Second, the difficult separation and recovery of TiO₂ powders from waste water (**Christophe et al. 1997; Zhu et al. 2000; Yu et al. 2002**). Considerable effort has been devoted to developing supported titanic catalysts that offer high active surface area as well as easy separation and removal from water (**Tanev et al. 1994; Walker et al. 1997**).

Silica has excellent adsorption properties due to its wide surface area caused by the presence of a network structure. The photodegradation of pollutant molecules on titania could be improved by an increase in the surface area. Therefore, the synergistic effects of photodegradation and adsorption on SiO₂-TiO₂ composites have been investigated (**De et al. 2008; Hu et al. 2001**). Because sol-gel derived titania is usually less porous, mesoporous titania has been prepared by introducing the appropriate template, such as a block copolymer (**Pan et al. 2011**), as a chelating agent into titania solution. The oxidants generated on titania surfaces barely diffused out of the mesopore to efficiently attack the substance inside the pores, which resulted in high reactivity (**Shiraishi et al. 2005**). In addition, the incorporation of silica into mesoporous titania improved its thermal stability (**He et al. 2010**). However, as far as we could ascertain, the kinetic approach using photodegradation and adsorption with a SiO₂-TiO₂ composite has not been reported.

In the present study, we aim to use a novel route to prepare the silica–titania nanocomposite catalysts. SiO₂-TiO₂ composite catalysts were synthesised by the sol-gel method using a new ethoxylated sulphanilamide as a chelating agent. The simultaneous photodegradation and adsorption behaviours of trichlorophenol (TCP) on a composite in the liquid phase were investigated under UV irradiation. A numerical evaluation for the photodegradation of TCP was also conducted.

2. Experimental

2.1. Synthesis of ethoxylated sulphanilamide oligomer (S)

Sulphanilamide was ethoxylated with 20 ethylene oxide units to give the ethoxylated sulphanilamide (S). The reaction was performed as follows: sulphanilamide was charged into a closed reaction vessel with 0.3 g sodium metal ("Na metal") as a catalyst and heated to 150 – 180 °C with continuous stirring while passing a stream of nitrogen gas through the system for 2 minutes then replacing the nitrogen with an ethylene oxide stream. After the reaction was completed, the apparatus was filled with nitrogen and cooled, and the reaction vessel was weighed. The difference in weight indicated the amount of the ethylene oxide consumed in the reaction, from which the number of moles of ethylene oxide was calculated (Hreczuch et al. 2001; Al-Sabagh et al. 2004; Sheu et al. 1995). The product was then neutralised with HCl, dissolved in isopropanol, then salted out with supersaturated NaCl solution. The organic layer was then separated, and the isopropanol was distilled off. The obtained ethoxylated product showed a brown viscous liquid appearance. The synthesis, evaluation and identification of the ethoxylated sulphanilamide have been described elsewhere by Mohamed and his co-workers (Mohamed et al. 2014).

2.2. Synthesis of Silica and Silica-Titania catalysts

SiO₂-TiO₂ nanocomposites were synthesised by the sol-gel method using tetraethyl orthosilicate (TEOS, 98% Aldrich) and titanium isopropoxide (TIP, 97% Aldrich) as the SiO₂ and TiO₂ sources, respectively, in acidic solution (pH=2). Herein, a novel ethoxylated sulphanilamide of molecular weight 1053 was used for the first time to prepare nanocomposite catalysts. In a typical synthesis, 4 g of the prepared ethoxylated sulphanilamide was added to 30 ml of water. After stirring for a few minutes at room temperature, a clear solution was obtained. The required amount of HCl was then added, and the solution was stirred for another 2 h. Then, 9 g of tetraethyl orthosilicate and titanium isopropoxide was added, according to the calculated molar ratios, to obtain 5, 10, 15 and 20 % Ti. The resulting mixture was stirred for 24 h at room temperature. The solid product was recovered by filtration, washed several times with water, and dried overnight at 100 °C. The sample was calcined at 540 °C with a heating ramp of 1°C to remove the organic template. Pure SiO₂ was synthesised using the same procedure mentioned above without adding titanium isopropoxide.

2.3. Characterisation

The materials were characterised by N₂ adsorption-desorption isotherms at -196 °C, which were obtained with a (NOVA 3200 apparatus, Quantachrome Corporation, Boynton Beach, Florida, USA). The samples were previously outgassed under vacuum at 300 °C overnight. The surface areas (S_{BET}) were calculated from multi-point at relative pressure (P/P₀) ranging from 0.05 to 0.30. The particle size distribution was calculated by the Barrett, Joyner and Halenda (BJH) method using the adsorption branch of the isotherms. VI-t plot was constructed using the adsorption branches according to the de Boer method. X-ray diffraction was recorded on a Bruker D8 Advance X-ray Diffractometer with Cu K α radiation ($\lambda = 1.5418 \text{ \AA}$).

The FTIR studies were performed using AT1 Mattson model Genesis Series (USA) infrared spectrophotometer adopting the KBr technique. For all samples, the KBr technique was performed approximately in a quantitative manner because the weight of the sample and that of KBr were always kept constant. The Brønsted and Lewis acidity of all catalyst samples were analysed by infrared spectroscopy using pyridine as the basic probe molecule on self-support wafers with a density of 7 mg/ cm³. The samples were activated at 300°C for 3 h under a vacuum of 10⁻⁴ Pa. Pyridine was adsorbed for 30 minutes at a room temperature after desorption at 150°C for 30 minutes under a vacuum of 10⁻⁴ Pa. The FTIR spectra of the adsorbed pyridine were recorded in the range of 1450-1550 cm⁻¹.

The ¹H-NMR spectra were measured in CDCl₃ using a Jeol ECA 500 MHz NMR spectrometer at 500 MHz. The measurements were performed at the National Research Centre. The DSC-TGA analyses were conducted for all samples using a simultaneous DSC-TGA SDTQ 600, USA under N₂ atmosphere, with a heating rate of 10°C min⁻¹. The morphology of the samples was studied with a Jeol TEM -1230 transmission electron microscope, 120 kW, 600,000 magnification, Japan.

2.4. Photolysis and photocatalysis experiments

A 500 cm³ volume of an aqueous solution containing 100 ppm of high purity 2, 4, 6-TCP was subjected to UV irradiation using a 6 watt lamp at a wavelength of 254 nm. All photodegradation experiments were conducted in a batch reactor at pH 5.3. The UV lamp was placed in a cooling silica jacket and placed in a jar

containing polluted water. A 0.1 g/L concentration of catalyst was suspended in the solution with a magnetic stirrer at a controlled reaction temperature of 25°C during the experimental period. In all cases, air was bubbled through the reaction mixture to ensure a constant dissolved O₂ concentration. At different irradiation time intervals, samples of the irradiated water were withdrawn for analysis using a Perkin Elmer high performance liquid chromatograph (series 200) with a photodiode array UV detector and a C₁₈ column. The mobile phase was acetonitrile/water (60:40) injected at a rate of 1.0 ml min⁻¹.

The concentration of the Cl⁻ and acetate ions produced in the solution during the photodegradation was determined by ion chromatography (IC Dionex-pac) using an AS14 column with an eluent of a 2:7 sodium carbonate:sodium bicarbonate mixture and a flow rate of 1.2 ml min⁻¹.

3. Results and Discussion

3.1. Characterisation of the synthesised ethoxylated sulphanilamide (S)

The chemical structure and the molecular weight of the prepared sulphanilamide are shown in Figure 1 and are confirmed by the FTIR and ¹H NMR spectra.

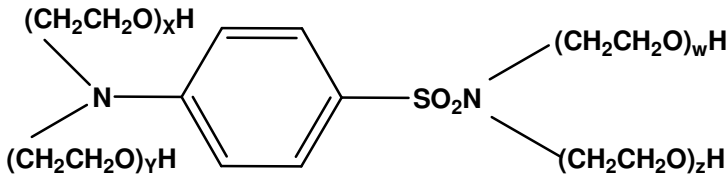
Sulphanilamide	Chemical Structure	Molecular Weight
S		1053

Fig. 1. Designation and molecular weight of the ethoxylated sulphanilamide (S)
 Where $x + y + w + z = 20$ units

3.1.1. FTIR spectrum

The FTIR spectrum of the synthesised ethoxylated sulphanilamide (S) showed absorption bands at 2876 and 1456 cm⁻¹, characteristic of stretching and bending vibrations of the methylene groups, respectively. The peak at 1106 cm⁻¹ is due to C-O stretching, indicating the formation of an ether bond due to the condensation of ethylene oxides. The band at 3384 cm⁻¹ is characteristic of the OH group of the ethylene oxide units. These results, together with the fact that the peak of NH₂ attached to the benzene ring and that of NH₂ attached to the sulphonate group (SO₂NH₂) disappeared, confirmed the investigated structure (Mohamed et al. 2014).

3.1.2. ¹H NMR spectrum

The ¹H NMR spectrum of the synthesised compound (S) showed different bands at δ (ppm): (4.52-4.53, 1H, OH), (3.17, 2H, SO₂N CH₂CH₂O), (3.19-3.27, 2H, SO₂N CH₂CH₂O CH₂-CH₂), (3.32-3.56, 2H, N CH₂CH₂O), (6.66-6.69, H_a Ar) and (7.45-7.48, H_b Ar). The data confirmed the expected hydrogen proton distribution of the synthesised compound.

3.2. N₂ physisorption

N₂ adsorption-desorption isotherms and surface parameters were conducted to investigate the surface morphology and physical properties of the composite samples. Figs. 2a and 2b display the N₂ adsorption-desorption isotherms and the pore size distribution calculated by the BJH method. Table 1 summarises the surface area and porosity results of the examined SiO₂-TiO₂.

The obtained isotherms for the prepared SiO₂ and SiO₂-TiO₂ nanocomposite samples are type I with H4 type hysteresis loops, which indicate microporosity. H4 represents an extreme type in the former; the adsorption and desorption branches are almost parallel over an appreciable range of the gas uptake. The isotherm is nearly horizontal over a wide range of relative pressure. Such H4 type hysteresis loops indicate the presence of slit-shaped pores according to the IUPAC classification (Sing et al. 1985).

The surface areas of the silica-titania samples increase with the addition of Ti compared with Pure SiO₂, which has a surface area of 289 m² g⁻¹. This may be due to the incorporation of TiO₂ into the SiO₂ framework. The S_{BET} increases to 10 %Ti-Si, which has a surface area of 374 m² g⁻¹. The S_{BET} then slightly decreases to 327

$\text{m}^2 \text{g}^{-1}$ for the 20 % Ti-Si sample. This may be due to the inclusion of titanium oxide particles in the pore system of the silica. Additionally, the total pore volume increases from 0.163 to $0.249 \text{ cm}^3 \text{ g}^{-1}$, indicating the formation of new porous structures.

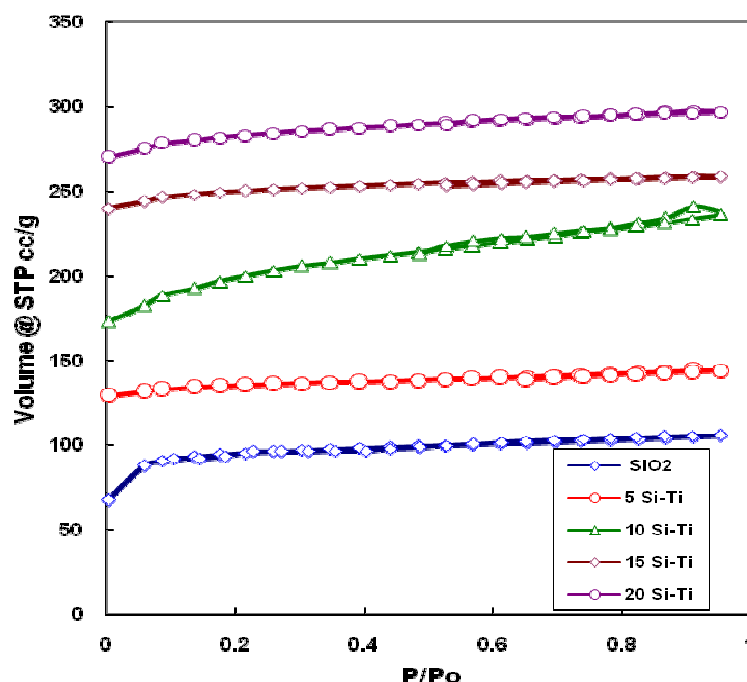


Fig. 2a. N_2 adsorption-desorption isotherms of SiO_2 and $\text{SiO}_2\text{-TiO}_2$ nanocomposite samples.

Table 1: Surface parameters of the SiO_2 and $\text{SiO}_2\text{-TiO}_2$ nanocomposite samples.

Catalyst Name	Surface area S_{BET} ($\text{m}^2 \text{g}^{-1}$)	V_p ($\text{cm}^3 \text{g}^{-1}$)	S_t ($\text{m}^2 \text{g}^{-1}$)	S_{micro} ($\text{m}^2 \text{g}^{-1}$)	S_{meso} ($\text{m}^2 \text{g}^{-1}$)	V_{micro} (ml g^{-1})	V_{meso} (ml g^{-1})	Average pore radius (\AA)
SiO_2	289	0.163	290	264	26	0.132	0.031	11.27
5 % Ti-Si	313	0.177	311	291	20	0.151	0.026	11.28
10 % Ti-Si	374	0.249	375	287	88	0.136	0.113	13.29
15 % Ti-Si	343	0.199	342	318	24	0.170	0.029	11.57
20 % Ti-Si	327	0.197	328	313	15	0.176	0.021	12.04

The V_t -t plots were constructed on the basis of the adsorption branches for each of the catalyst samples investigated at liquid nitrogen temperature and these are shown in Fig. 2b. The nitrogen t-curve used was suggested by de Boer et al. (Lippens et al. 1964). The total surface area ($S_t \text{ m}^2 \text{ g}^{-1}$) was obtained from the slope of the initial straight line that passes through the origin, and the values are given in Table 1, column 4. The plots demonstrate that the pore system consists mainly of micropores with a very minor fraction of mesopores, as indicated by the strong downward deviations from the initial straight lines passing through the origin, which reflects the predominance of micropores. Therefore, the pore structure analysis of all samples was performed using the MP-method developed by Mikhail and Brunauer (Mikhail et al. 1968) to calculate the surface (S_{micro}) and the volume (V_{micro}) of the micropores present, and the values are given in columns 5 and 7 of Table 1. The fractions of the surface and volume of mesopores (S_{meso} and V_{meso}) were calculated from the differences between those of the micropores (S_{micro} and V_{micro}) and the total surface area (S_t), as well as the total pore volume (V_p), and the values are given in columns 6 and 8, respectively. The 10% Ti/ SiO_2 showed the greatest mesoporous surface area ($S_{\text{meso}} = 88 \text{ m}^2 \text{ g}^{-1}$) and volume of mesopores ($V_{\text{meso}} = 0.113 \text{ cm}^3 \text{ g}^{-1}$).

In conclusion, the results of the pore structure characteristics revealed that almost all of the total pore system is composed of micropores, as indicated from the strong downward deviations in the V_t -t plots, which specify that the normal multilayer adsorption is hindered due to the presence of micropores. This hindrance is illustrated by the higher values of the fraction located in the mesopores (S_{meso}/S_t) with a much lower value of the fractions located in mesopores (S_{meso}/S_t) (Hanafi et al. 2014).

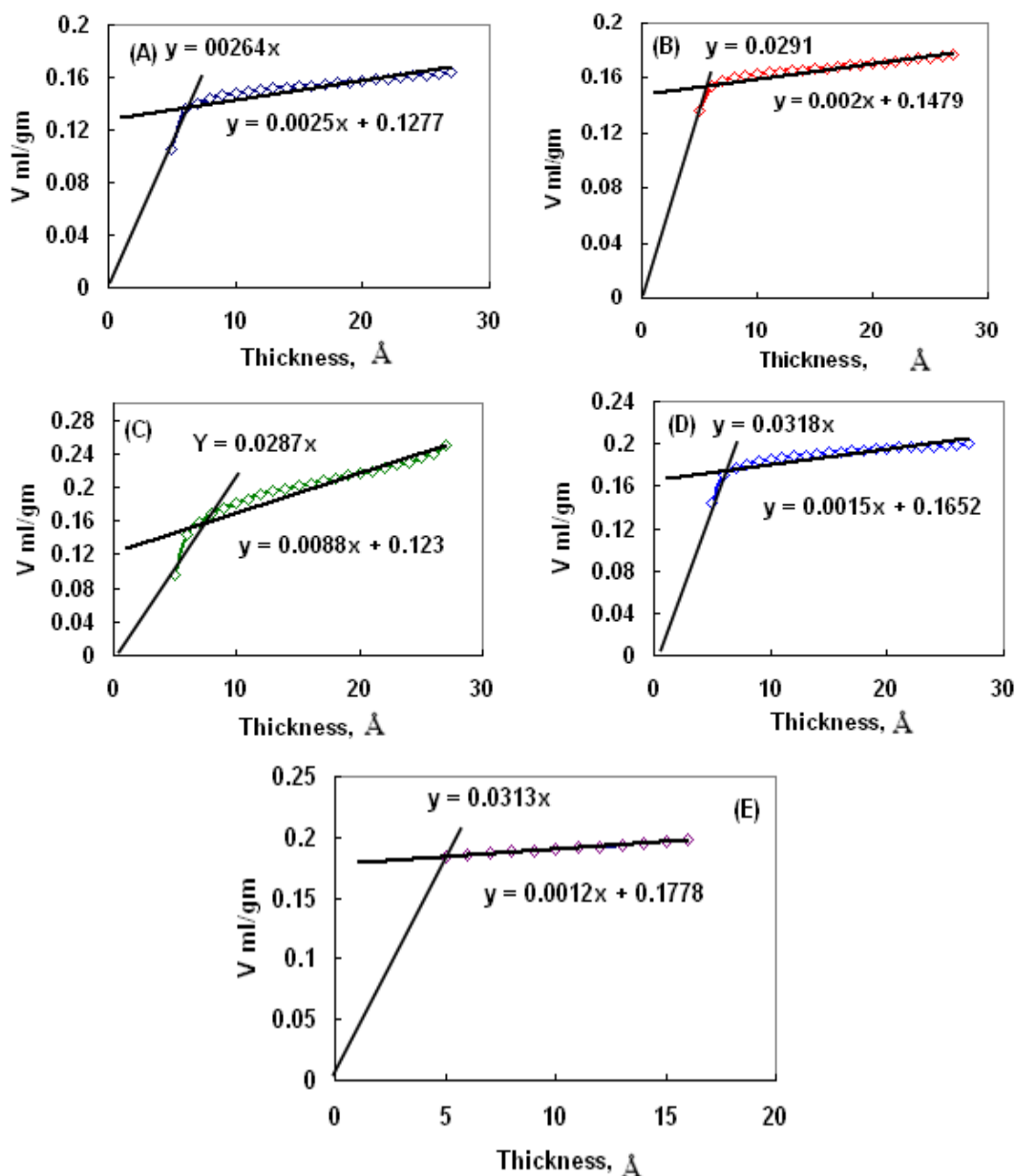


Fig. 2b. V_t - t plot for SiO_2 (A) and SiO_2 - TiO_2 nanocomposite samples: 5% (B), 10% (C), 15% (D) and 20% TiO_2 (E).

3.3. XRD analysis

To identify the crystalline phases present in the samples, the X-ray diffraction analyses of the synthesised pure silica and silica-titania nanocomposite catalysts were performed. The XRD patterns (Fig. 3) showed a broad diffraction band between 15° and 40° 2θ in all samples under study, which is attributed to the amorphous pattern of the SiO_2 and TiO_2 . No diffracted lines corresponding to SiO_2 and TiO_2 appeared.

This indicated that the silica and titania phases in the prepared composites exist as amorphous states. These results demonstrated the existence of well-dispersed titanium in the amorphous silicate framework (**Katsunori et al. 1999**; **Viswanath et al. 2001**; **Hu sing et al. 2002**). Additionally, it may be segregated as an amorphous phase in the silica matrix.

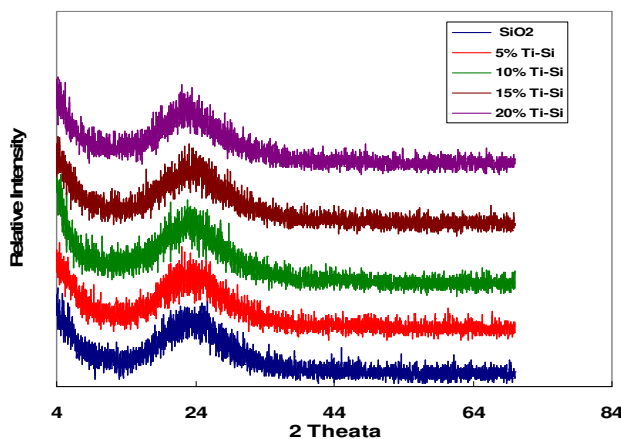


Fig. 3. X-ray diffraction analysis of the SiO_2 and $\text{SiO}_2\text{-TiO}_2$ nanocomposite samples.

3.4. FT-IR spectroscopy

The FTIR spectra of the silica-titania composites are characterised by a specific band assigning a titanium or silicon bond in the framework. The peak at the wave number of 800 (**Brinker et al. 1990**) or 810 cm^{-1} (**Marth et al. 1992**) corresponds to the symmetric vibration of Si–O–Si. The peak at 1080–1105 cm^{-1} (**Duran et al. 1986**) is for asymmetric ν (Si–O–Si) stretching vibration, and 940–960 cm^{-1} is for the Si–O–Ti vibration (**Dutoit et al. 1995**), although the exact positions of the bands indicating symmetric or asymmetric stretching vibration of Si–O–Si and Si–O–Ti vibration vary slightly in the literature. Fig. 4 shows the FT-IR spectra of pure and silica-incorporated titania nanoparticles with different Ti percentages. The absorption peaks at 600–900, 1000–1200, and 960 cm^{-1} are attributed to Ti–O, Si–O–Si, and Ti–O–Si, respectively (**Rubio et al. 1997**; **Kim et al. 2003**). The absorption band at 609 cm^{-1} is attributed to the Ti–O stretching vibrations of TiO_2 (**Lee et al. 2003**). This peak could be clearly detected in Fig. 5 at 611, 613 and 620 cm^{-1} in all samples, except pure silica, and its intensity increased with increasing Ti content. When the silicon content was over 30%, the distinct band for the Ti–O–Si vibration (960 cm^{-1}) was observed. The band for the asymmetric ν (Si–O–Si) stretching vibration was observed for all samples, and its intensity increased with increasing silicon content. From the results of the XRD and FT-IR, it is clear that the silica exists as an amorphous phase. The peaks observed at 1628 and 3431 cm^{-1} in Fig. 5 could be assigned to bending and stretching of O–H, respectively, (**Kang et al. 2003**) for the O–H stretching of the defect Si–OH groups and residual water in pure calcined silica, as well as the synthesised Ti-silica samples. This water band increased with increasing the Titanium oxide content.

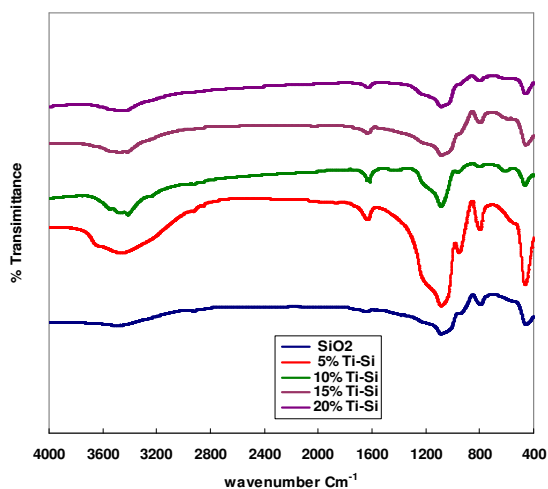


Fig. 4. FT-IR analysis of the SiO_2 and $\text{SiO}_2\text{-TiO}_2$ nanocomposite samples.

The FTIR-spectra of the adsorbed pyridine on the SiO₂ and SiO₂-TiO₂ nanocomposite catalysts are shown in Figure 5. The vibration bands in the 1400-1580 cm⁻¹ regions of the IR spectrum of the chemisorbed pyridine could distinguish between the Brønsted and Lewis acid sites. The sharp peak at 1530 cm⁻¹ is attributed to the C–C stretching vibration of the pyridinium ion and indicates the presence of pyridine adsorbed on Brønsted acid sites. The pyridine adsorption on Lewis acid sites is indicated by another peak at 1460 cm⁻¹, arising from the C–C stretch of a coordinative bonded pyridine complex (Barzetti et al. 1996). The 10% Ti-Si catalyst showed the highest acidity of the samples under investigation.

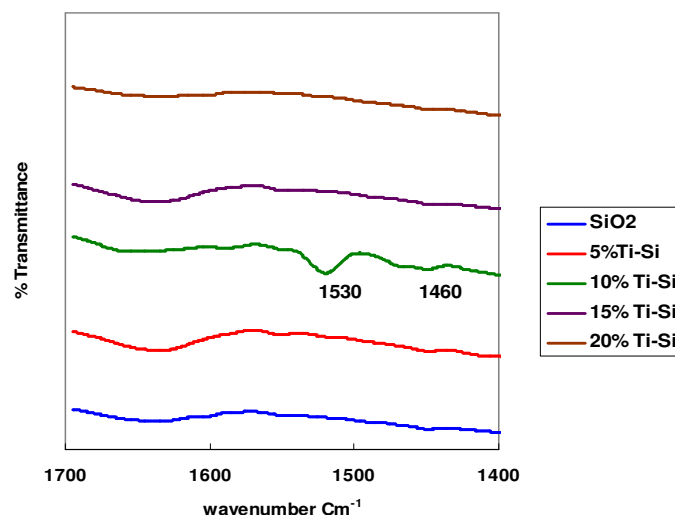


Fig. 5. FTIR-spectra of adsorbed pyridine on the catalysts under investigation.

3.5. Thermal analysis

In Figs. 6 (a & b), a quantitative estimation of the content losses of the synthesised silica-titania samples are measured using thermal gravimetric analysis (TGA) and differential scanning calorimetry (DSC) under N₂ flow. With an increase in temperature, the sample gradually loses weight (ca.13-15%) in the temperature range 73-120 °C due to desorption of physisorbed water. The pure silica and silica-titania nanocomposite are thermally stable up to 800°C. There is no loss in TGA thermogram above 500°C, which can be related to the organic oligomer template material (S) and indicates that the calcination conditions are optimal to complete the removal of the oligomer template from the silica and silica-titania pores.

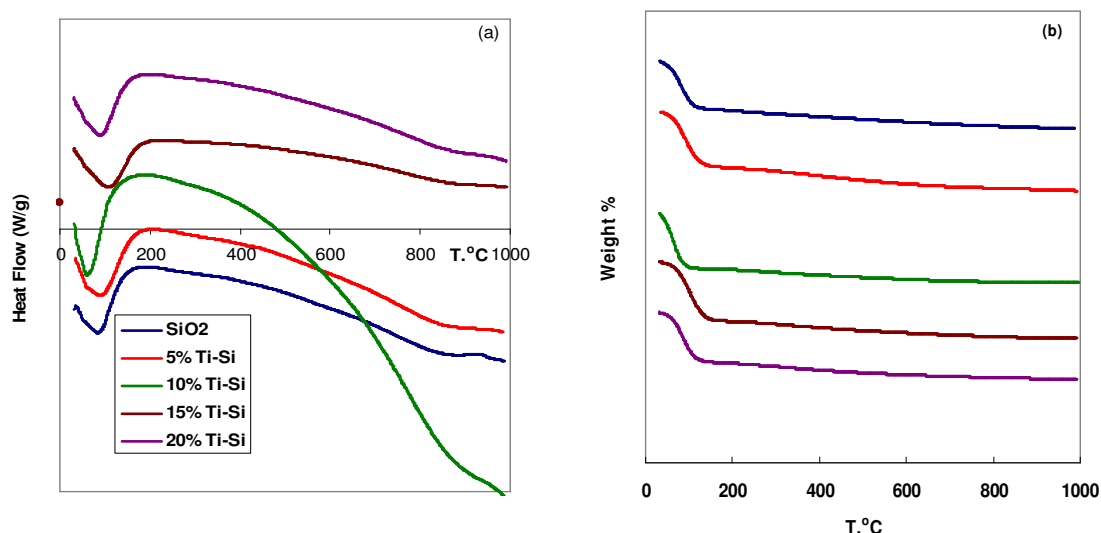


Fig. 6. DSC (a) and TGA (b) of the SiO₂ and SiO₂-TiO₂ nanocomposite samples.

3.6. TEM micrographs

The morphology of the synthesised catalysts was further observed with TEM micrographs, as shown in Fig. 7. Pure SiO₂ micrographs show uniform distribution of the silica particles, and the average particle size of Si = 8 nm. For 5% TiO₂-SiO₂, the network increased due to the incorporation of Ti in the silica framework, as

evidenced from the surface, X-ray and FT-IR. Additionally, its EDX micrographs showed the presence of Ti, as well as Si and O. The TEM micrograph of the 10% TiO₂-SiO₂ showed scattered black spots, which are presumed to be the composite of SiO₂-TiO₂. The TEM image clearly showed spherical nanoparticles with almost uniform diameter with a narrow range distribution. The average diameter was approximately 20 nm. A composite microstructure for the catalysts is likely formed with no definite morphology ordering because the TiO₂ is well-dispersed titanium in the amorphous silicate framework. After increasing the % Ti to 15 %, a particle growth is clearly observed in the TEM micrograph (Fig. 7d, e) as a result of composite swelling due to the removal of the hydroxyl group by incorporation of TiO₂, as clearly observed in the FT-IR section (Fig. 4).

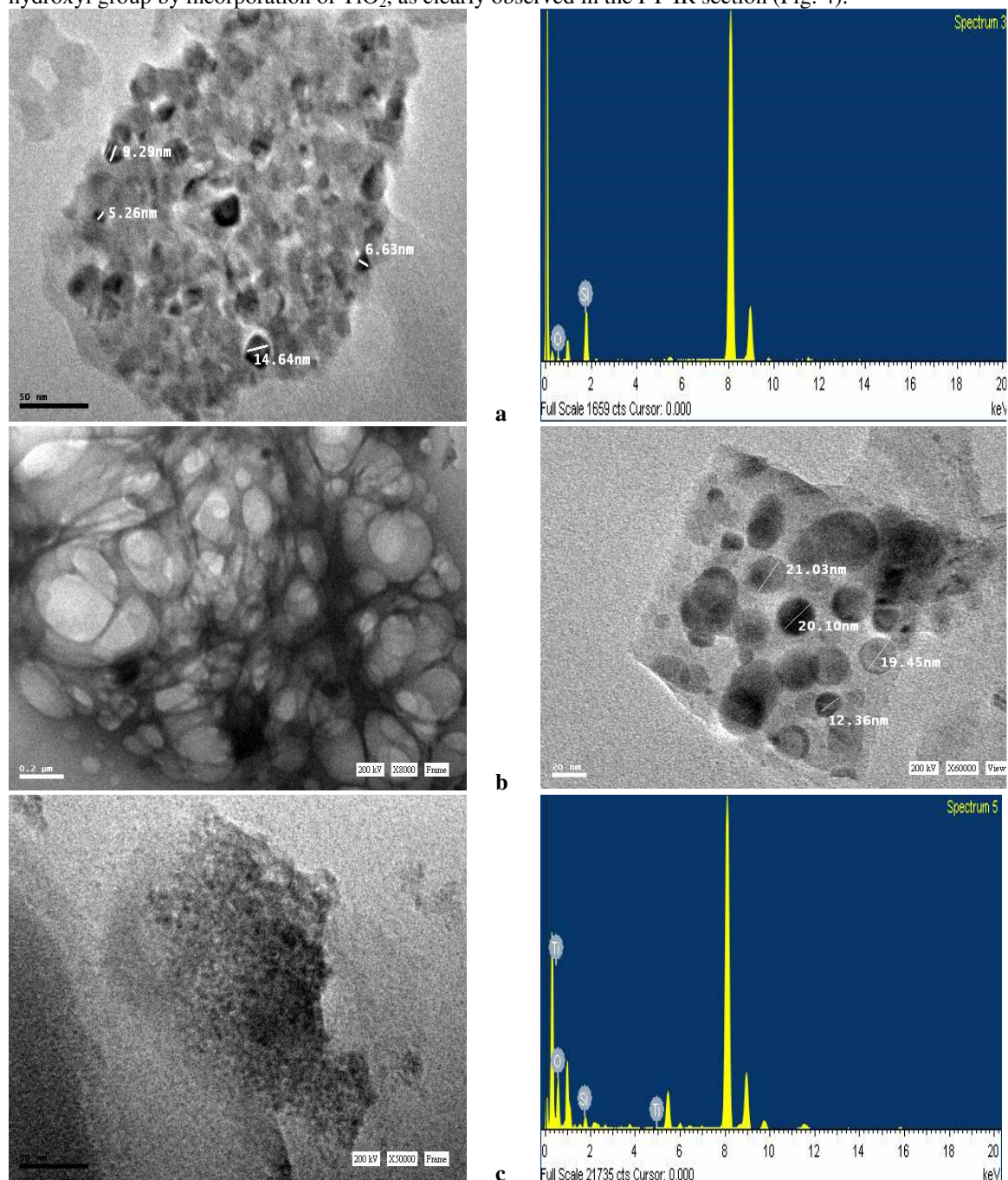


Fig. 7a. TEM and EDX of (a) SiO₂ and SiO₂-TiO₂ samples with different Ti percentages (b) 5%, and (c) 10%.

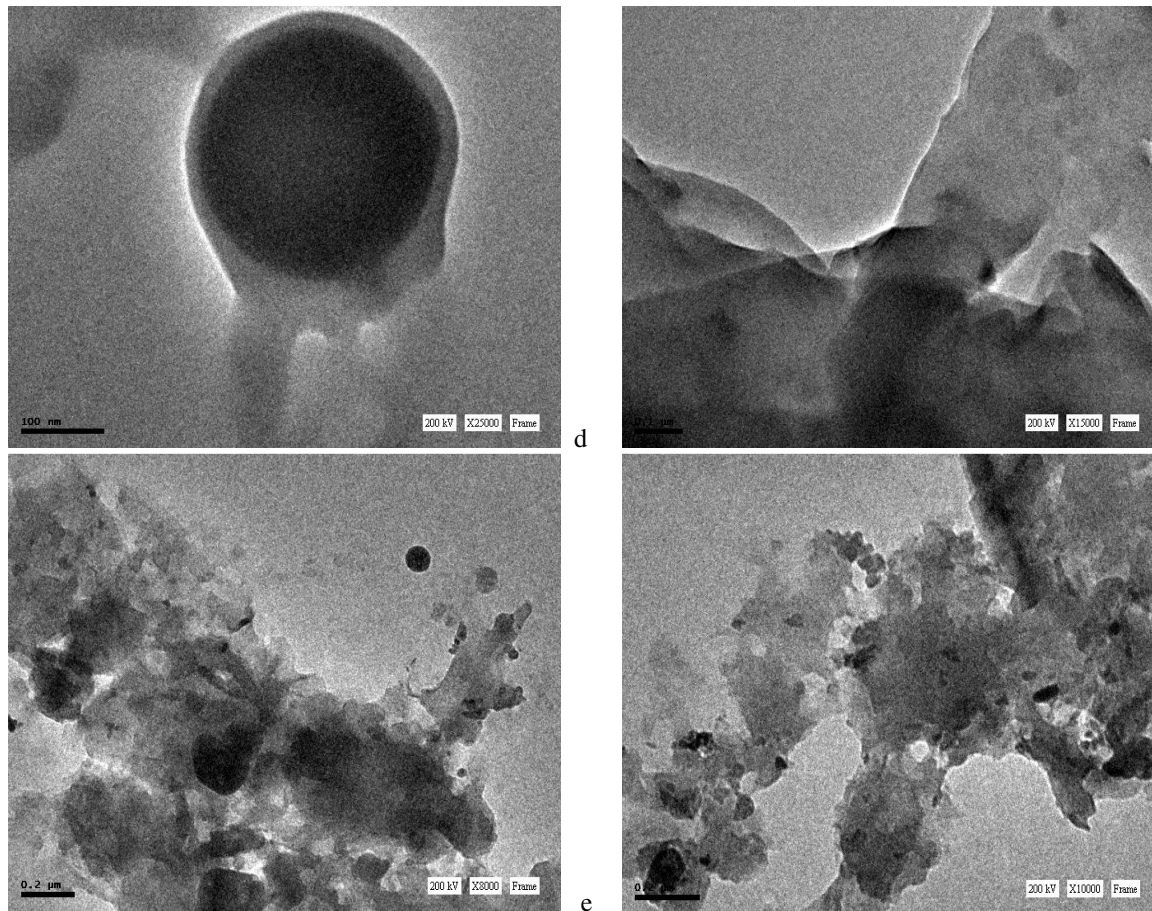


Fig. 7b. TEM and EDX of (a) SiO_2 and $\text{SiO}_2\text{-TiO}_2$ samples with different Ti percentages (d) 15 % and (e) 20 %.

3.7. Photocatalytic activity:

The photodecomposition and the photocatalytic degradation of 100 ppm 2, 4, 6-trichlorophenol (2, 4, 6-TCP) using a series of mesoporous $\text{SiO}_2\text{-TiO}_2$ catalysts with different titania ratios under UV light with $\lambda_{\text{max}} = 254 \text{ nm}$ are shown in Fig. (8).

The removal efficiency after 90 min irradiation time increases according to the order of 10% $\text{Ti-SiO}_2 > 5\% \text{ Ti-SiO}_2 > 20\% \text{ Ti-SiO}_2 > \text{SiO}_2 > \text{photolysis} > 15\% \text{ Ti-SiO}_2$ Fig. 8. The 10% Ti-SiO_2 catalyst is generally the most active catalyst. It exhibits high activity during the initial 20 min of irradiation, beyond which the photodegradation stays constant until 90 min of irradiation.

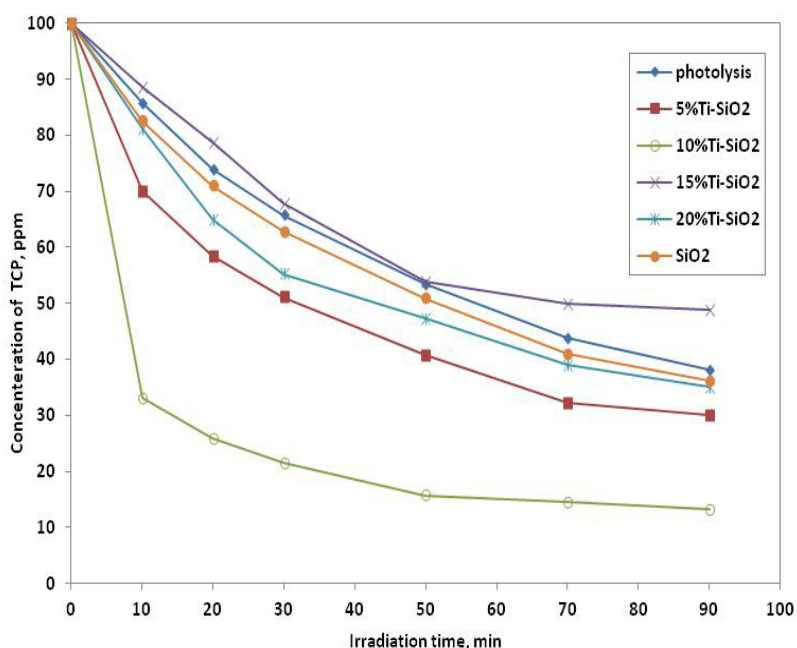


Fig. 8. Photocatalytic degradation of 100 ppm 2,4,6-TCP on different mesoporous SiO₂- TiO₂catalysts using UV irradiation at 254 nm.

This activity is also attributed to its high textural properties, as shown in Table 1, as well as its highest acidity. Overall, based on the previous literature, the degradation of the substance depends on the adsorption of the substance on the catalyst. Substances that are adsorbed strongly degrade faster (Tanaka et al. 2000). This is a clear indication that the reaction must occur on the catalyst surface itself. No dark adsorption was observed using pure silica, which means that silica-loaded titania has increased adsorption capacity and generally a higher efficiency compared with pure silica. It has been reported that surface bond-conjugated SiO₂/TiO₂ photocatalyst has higher photoactivity than TiO₂ powder in eliminating azo dyes (Chun et al. 2004). The incorporation of TiO₂ with SiO₂ is an effective method to improve the photocatalytic activity because the phase transformation from anatase to rutile is inhibited due to the enhanced thermal stability of the SiO₂-TiO₂ mixed oxide system (Sayilkan et al. 2007). The 10% Ti-SiO₂ catalyst acquires the highest surface area, 374 m²/g, and the largest pore radius, 13.3 Å, so it has the highest TCP adsorptive capability of the tested catalysts. The maximum concentration of adsorbed trichlorophenol reached 60 ppm after 60 min in the dark, as shown in Fig. 9.

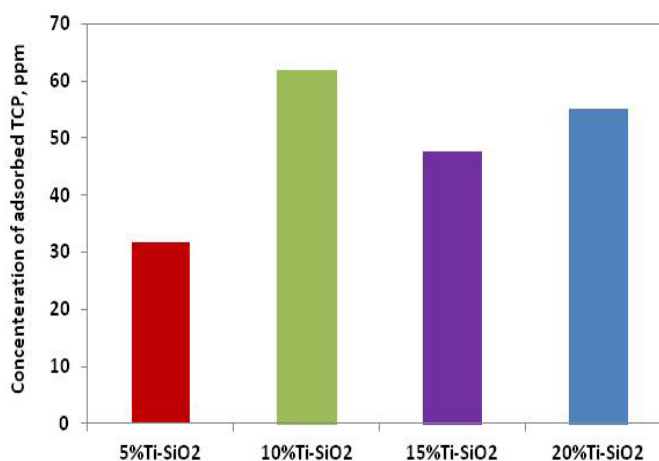


Fig. 9. 2,4,6-TCP adsorbed on different catalysts after 60 min the dark.

However, the total pore volume of the 10 % Ti-SiO₂ catalyst is 0.249 cm³g⁻¹. This has a positive effect on the diffusion of trichlorophenol through the catalyst pores. Generally, the difference in pore volume and surface area

in Ti-SiO₂ catalysts is attributed to the dispersion of TiO₂ inside the supports, which causes partial blockage of the pores (Bhattacharyya et al. 2004).

The chloride evolution resulting from TCP degradation after 90 min irradiation time increases according to the order: SiO₂ > 15% Ti-SiO₂ > 5% Ti-SiO₂ > 20% Ti-SiO₂ > photolysis > 10% Ti-SiO₂ (Fig. 10). This higher chloride concentration most likely inhibits the continuation of the photodegradation of TCP, so the catalyst becomes ultimately less active than the 10%Ti-SiO₂ catalyst. In general, chloride has a greater effect on adsorption of pollutants on the catalyst, causing its poisoning and decreasing the catalytic efficiency. Chloride ions absorb UV light, and they act as scavengers of hydroxyl radicals (Elsalamony 2010).

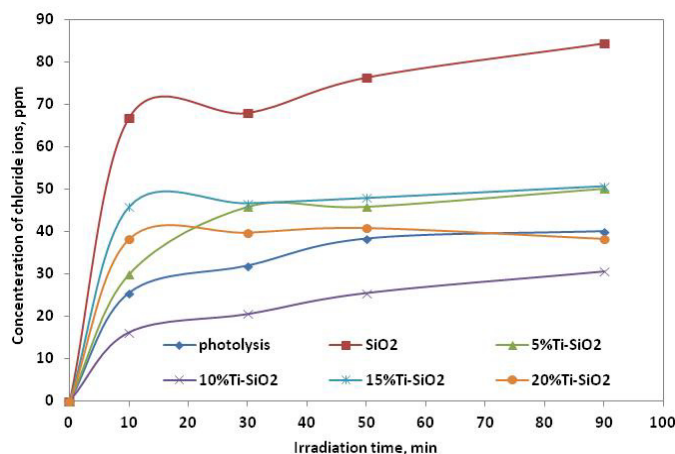


Fig. 10. Variation of [Cl⁻] in polluted water with the irradiation time.

Again, the photocatalytic activity of the 10%Ti-SiO₂ catalyst was confirmed from the FTIR spectra, and the two strong bands observed at 3441 and 1628 cm⁻¹ are characteristic for the O-H bending mode of the hydroxyl groups present on the surface due to moisture. These are crucial to the photocatalytic reactions because they can react with photoexcited holes generated on the catalyst surface and produce hydroxyl radicals (Ding et al. 2000), which are powerful oxidants.

3.8. TCP degradation mechanism

To investigate the degradation mechanism, the intermediate products during TCP degradation on mesoporous catalysts were determined by HPLC. The obtained data allowed for the qualitative and quantitative identification of these intermediates. Therefore, Fig. 11 showed the variation of intermediate concentrations formed during TCP degradation on photolysis and Ti-SiO₂ catalysts. The concentration of two major compounds increases with irradiation time, reaching a maximum and then decreasing gradually with a further increase of irradiation time. They were identified to be 3, 5-dichlorocatechol (3,5DCC) and 2,6-dichlorohydroquinone (2,6DCHQ). Evidently, the 3,5-dichlorocatechol is produced by replacing one of the ortho-Cl atoms with a hydroxyl radical in the TCP molecule, as shown in scheme 1a. A third intermediate, benzoquinone (BQ), appeared with a concentration increasing linearly from the beginning as a function of irradiation time.

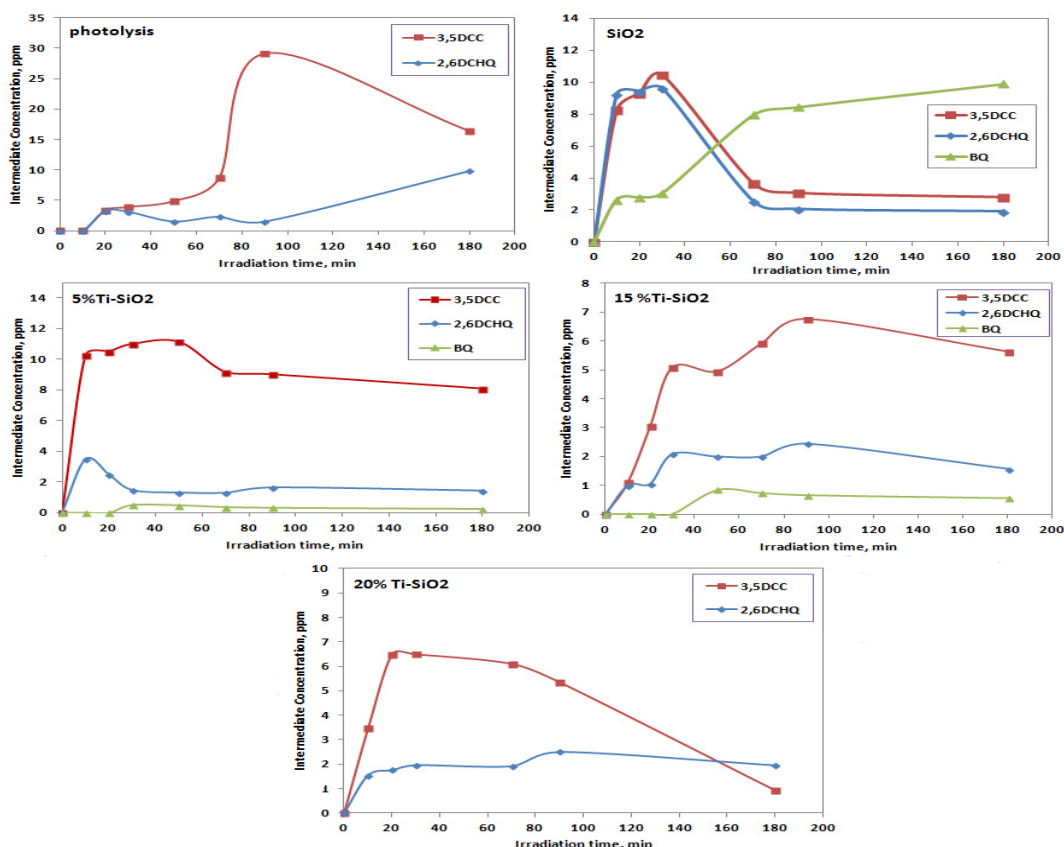


Fig. 11. Formation of 3,5-dichlorocatechol (3,5DCC), 2,6-dichlorohydroquinone (2,6DCHQ), and benzoquinone (BQ) during the photodegradation of TCP using UV light (photolysis), Ti-SiO₂ catalysts at pH 6 and with 100 ppm as an initial concentration.

In the photocatalytic degradation of TCP using the 10 % Ti-SiO₂ catalyst, two minor components possessed low concentrations, as shown in Fig. 12. They were identified as trichlorodihydroxybenzene (TCDHB) and trihydroxydichlorobenzene (THDCB). The first component is produced via the addition of a hydroxyl radical in the meta-position in the TCP molecule, whereas the latter component is produced by substitution of a Cl atom in the para-position in trichlorodihydroxybenzene (TCDHB) molecule by a new hydroxyl radical as shown in scheme 1b.

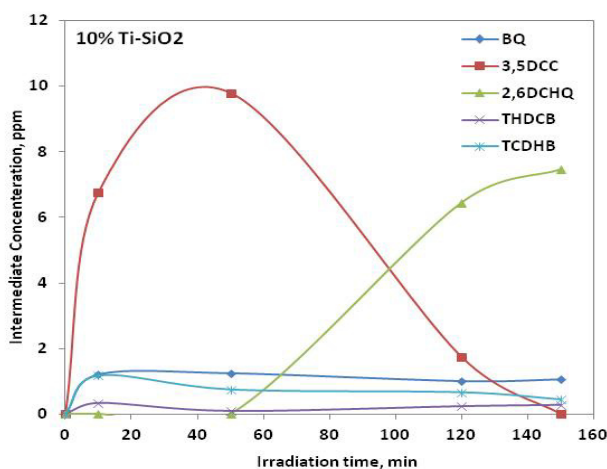
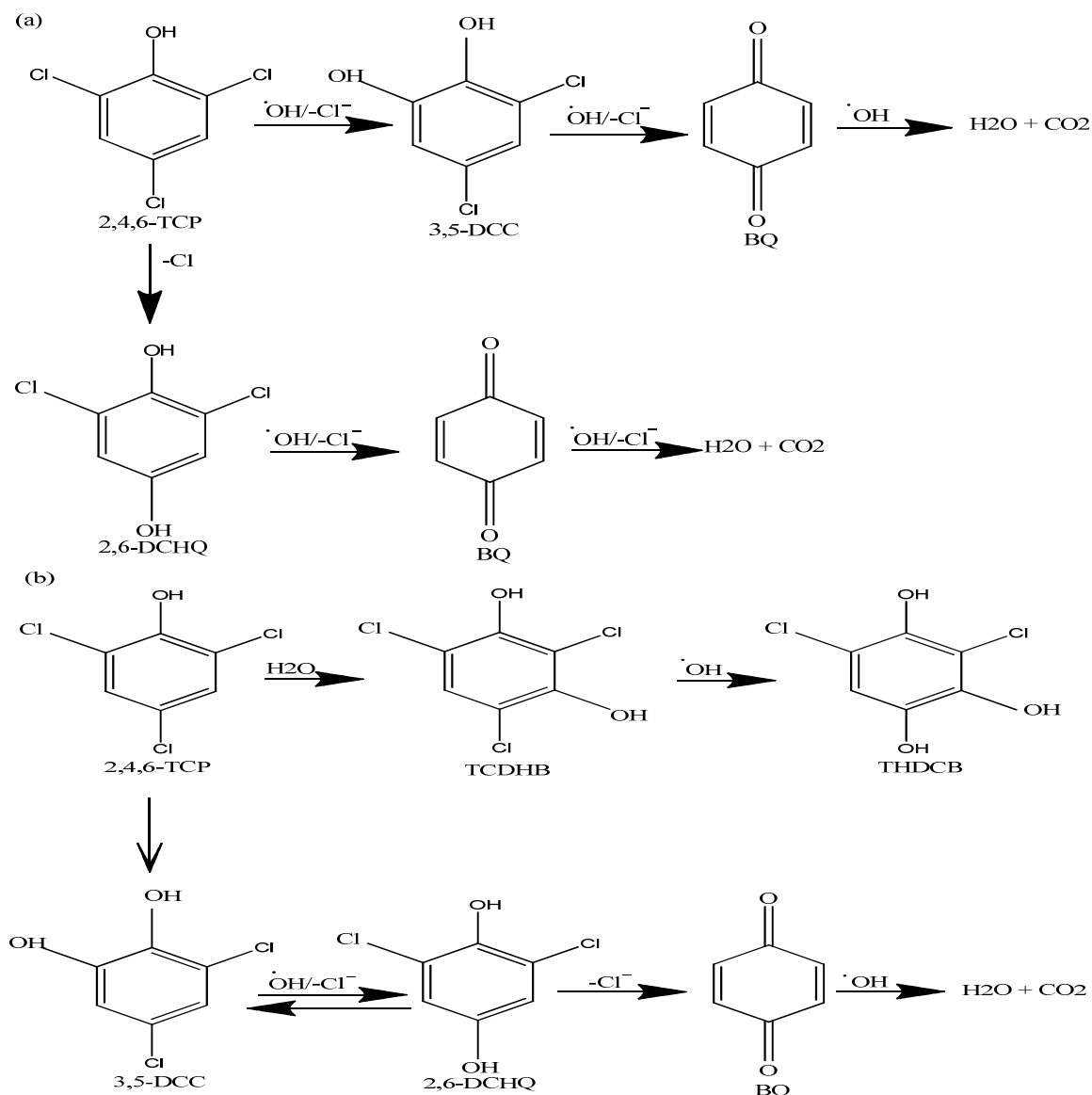


Fig. 12. Formation of dihydroxytrichlorobenzene (DHTCB), dichlorotrihydroxybenzene (DCTHB), 3,5-dichlorocatechol (3,5DCC), 2,6-dichlorohydroquinone (2,6DCHQ), and benzoquinone (BQ) during the photodegradation of TCP using 10% Ti-SiO₂ catalyst at pH 6 and with 100 ppm as an initial concentration.

The primary reactions of 2,4,6-TCP photodecomposition involve: a) hydroxylation of the aromatic ring, b) substitution of chlorine by OH and c) oxidation of the chlorinated hydroquinone to the corresponding quinone (Antonaraki et al. 2002).



Scheme 1. Photocatalytic degradation of TCP using (a) photolysis and Ti-SiO₂ catalysts and (b) 10% Ti-SiO₂ catalyst.

4. Numerical evaluation of TCP degradation

4.1. The Reaction Kinetics.

The photocatalytic degradation of organic pollutants generally follows the Langmuir-Hinshelwood mechanism (Ilyas et al. 2011; Herrmann 2005):

$$r = -\frac{dC}{dt} = k \frac{KC}{1 + KC}$$

Where k is the true rate constant, which depends on the mass of the catalyst, the flux of efficient photons, and the surface coverage. K is the adsorption constant, t is the time, and C is the concentration of the organic pollutant.

For low initial concentrations of pollutants, the term KC in the denominator can be neglected, and the photocatalytic oxidation rate approaches first order kinetics described by

$$r = -\frac{dC}{dt} = kKC = k'C$$

Where k' is the apparent rate constant, which is also known as the pseudo-first order rate constant. The integral form of the rate equation is

$$\ln \frac{C}{C_0} = -k' t \quad \text{or} \quad \ln \frac{C_0}{C} = k' t \quad (1)$$

Where C_0 is the initial concentration.

4.2. Mathematical model for the degradation of TCP with irradiation time

A numerical investigation has been performed to determine the relationship between the degradation of TCP and the irradiation time. The following second order polynomial (Eq. (2)) is the most suitable formula to describe the relation between C_0/C and the irradiation time t .

$$\left(\frac{C_0}{C} \right) = B_0 + B_1 t + B_2 t^2 \quad (2)$$

4.3. Evaluation of the constants in the above equations

The regression analysis was performed via the least square method, which minimises the variance of the unbiased estimators of the coefficients to estimate the coefficients of the equations (Hoffmann 2010; Weisberg 2005). Microsoft Excel 2007 was employed to determine the coefficients of the equations along with the statistical parameters that validate the results.

4.4. Evaluation of the results

- The coefficient results of these relations are depicted in Tables 2 and 3, together with the values of R squares, the calculated F ratio and the regression significance F, which assess the adequacy of the 'fitted' equation. Moreover, the values of the 95% confidence limits and the p-value, which validate the precision of the predicted regression coefficient, are shown.
- Regarding the R squared, which indicates the goodness of fit between the experimental values and the corresponding equations, tables 2 and 3 present high values for $R^2 > 0.9$ obtained for the above relations (1 & 2). This proves the adequacy of the corresponding equations for representing the experimental results. The high values of the calculated F ratio compared to the corresponding tabulated ones and the very small values of the significance $F < (\alpha = 0.05)$ indicate that there is a real relation between the independent irradiation time variable and the corresponding dependent response variable (LN (C_0/C) or C_0/C) for all the investigated cases. The low values of p depicted in Tables 2 and 3 indicate that all the recorded coefficients are significant. This is also manifested in the small values of the coefficients' limits in comparison with their corresponding ones, which means that they do not span zero as a value for the parameter. It could be concluded that the above equations, together with the corresponding recorded parameters, are statistically significant for all the investigated cases (Hoffmann 2010; Weisberg 2005).
- The pseudo-first order rate constants, which reflect the initial degradation rates for the investigated cases, are in the following order Table (2) & Fig. (13):
 $10 \%Ti O_2/SiO_2 \gg 5\%TiO_2/SiO_2 > 20 \%Ti O_2/SiO_2 > SiO_2 > \text{photolysis} > 15 \%TiO_2/ SiO_2$
- Figs (13) and Table (2) depict a linear relationship between the independent irradiation time variable and the corresponding dependent response variable (C_0/C) for the first three investigated cases. Additionally, the values of the B1 parameter, which reflect the degradation rate, are in the following order: $5\%TiO_2/SiO_2 > SiO_2 > \text{photolysis}$, in agreement with the above obtained results for the pseudo-first order rate constants.
- Figs (14) and Table (3) show the second order polynomial, which represents the relation between the independent irradiation time variable and the corresponding dependent response variable (C_0/C), for the last three investigated cases. The recorded values of B1, which reflect the initial degradation rate, are in the following order: $10 \%Ti O_2/SiO_2 \gg 20 \%Ti O_2/SiO_2 > 15 \%Ti O_2/SiO_2$, also in agreement with the above obtained results for the pseudo-first order rate constants.

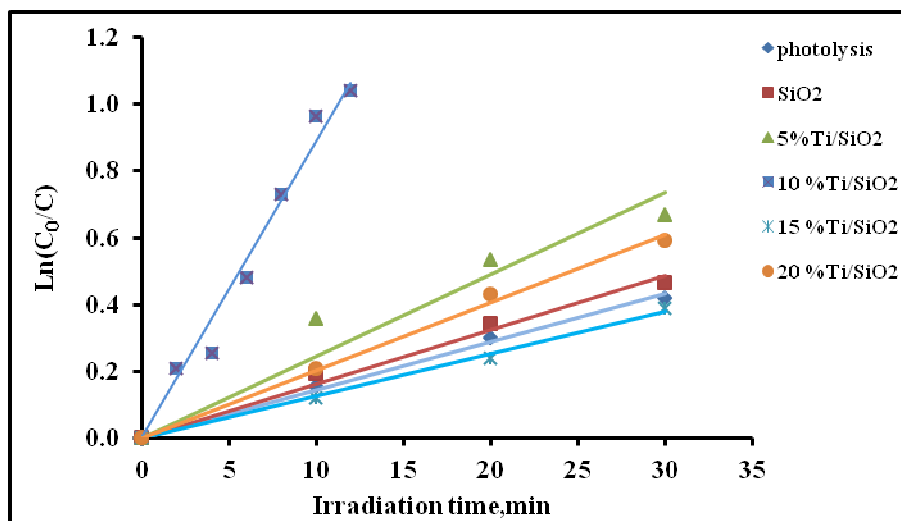


Fig. 13. Kinetics of the initial TCP photocatalytic degradation

Table 2. Pseudo-First Order Kinetics for the Degradation of TCP

Regression Statistics and Parameters	photolysis	SiO ₂	5% TiO ₂ /SiO ₂	10 %Ti O ₂ /SiO ₂	15 %Ti O ₂ /SiO ₂	20 %Ti O ₂ /SiO ₂
R Square	0.999	0.996	0.978	0.993	0.999	0.998
Calculated F Ratio	2074.9	672.4	135.2	850.1	2168.7	1888.7
Tabulated F Ratio	10.13	10.13	10.13	5.99	10.13	10.13
Significance F	4.816E-04	1.484E-03	7.317E-03	8.895E-07	4.608E-04	5.290E-04
Slope = k, min ⁻¹	1.439E-02	1.624E-02	2.458E-02	1.117E+01	1.260E-02	2.037E-02
k - Lower 95%	1.338E-02	1.425E-02	1.785E-02	1.024E+01	1.173E-02	1.888E-02
k - Upper 95%	1.539E-02	1.823E-02	3.131E-02	1.211E+01	1.346E-02	2.186E-02
P-value	2.329E-05	1.258E-04	1.367E-03	1.079E-07	2.180E-05	2.682E-05

$$^a D \% : \text{Degradation \% after 90 min of irradiation} = \frac{(C_0 - C_{90})}{C_0} * 100$$

5. Conclusion

A novel route has been introduced to prepare silica–titania nanocomposite catalysts, in which the SiO₂–TiO₂ catalysts were synthesised by the sol-gel method. The co-hydrolysis and condensation reaction of titanium isopropoxide (TIP) and tetraethoxysilane (TEOS) in acidic solution were conducted using a novel ethoxylated sulphanilamide. This synthetic method of silica–titania has resulted in a high degree of homogeneous titanium dispersion and a high specific surface area. XRD and FT-IR analyses showed that the TiO₂ can incorporate the amorphous silicate framework. The results of the activity test indicated that the 10%Ti-SiO₂ catalyst has the greatest photocatalytic activity towards 2,4,6- trichlorophenol photodegradation among the x%TiO₂-SiO₂ (x= 0, 5, 10, 15, 20) catalysts. Silica–titania prepared in this study had better photocatalytic performance than that of the commercial pure SiO₂ nanoparticles for the photodegradation of the 2, 4, 6 trichlorophenol (TCP). The Langmuir-Hinshelwood kinetic model provided a good fit to the initial photocatalytic degradation of the TCP compound used in this study. Additionally, the second order equation presented adequate relation between the amount (C₀/C) and the irradiation time. Both relations proved to be significant.

Acknowledgment

This work was supported by the Egyptian Petroleum Research Institute Labs and Instruments.

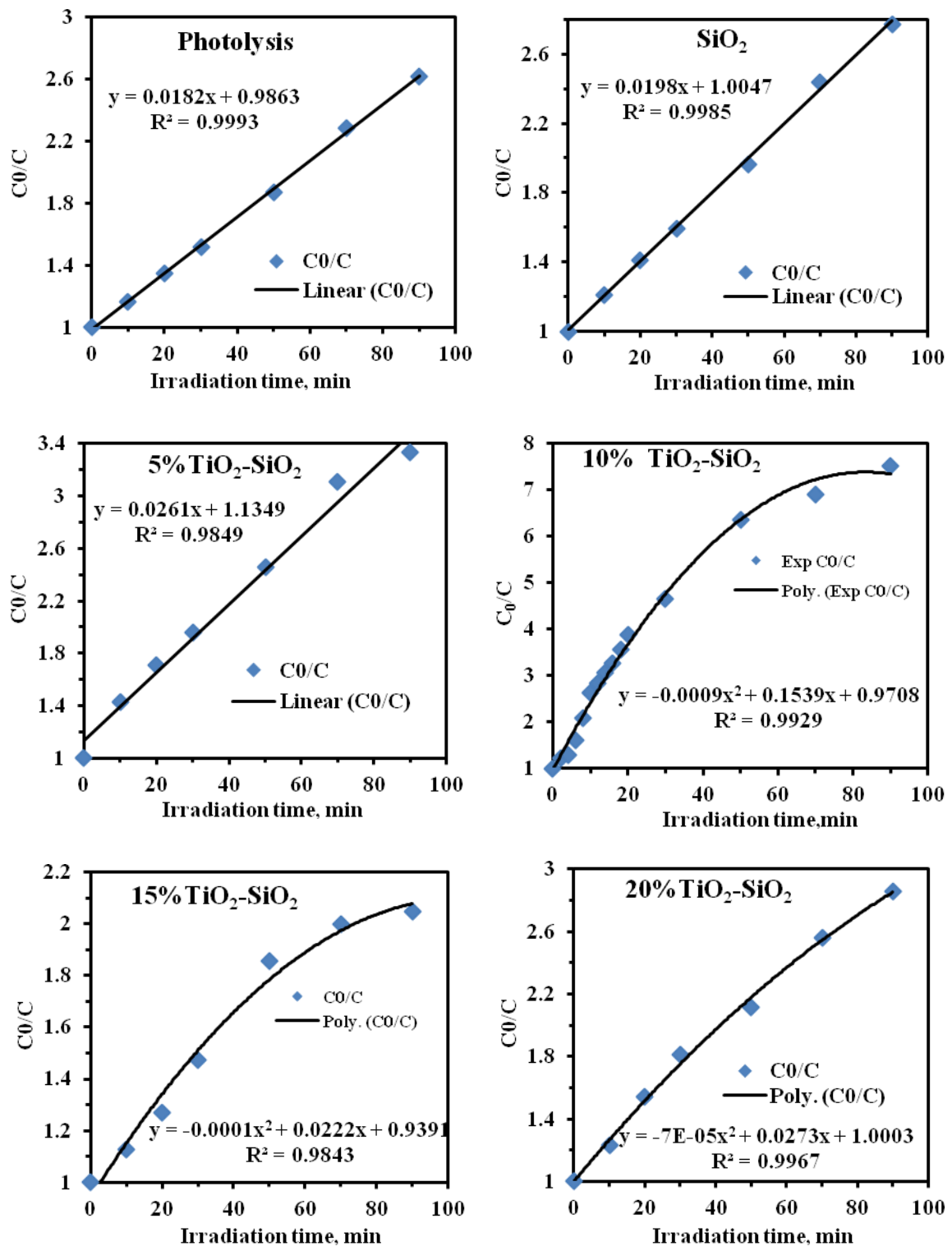


Fig. 14. The relationship between the degradation of TCP and the irradiation time

Table 3. Regression Statistics and Estimated Parameters for equation 2

Regression Statistics and Parameters		photolysis	SiO ₂	5% TiO ₂ /SiO ₂	10 % Ti O ₂ /SiO ₂	15 % Ti O ₂ /SiO ₂	20 % Ti O ₂ /SiO ₂
Regression Statistics	R Square	0.999	0.999	0.985	0.993	0.984	0.997
	Calculated F Ratio	7064.5	3397.6	325.5	843.3	125.2	597.2
	Tabulated F Ratio	6.608	6.608	6.608	3.885	6.944	6.944
	Significance F	4.518E-09	2.812E-08	9.612E-06	1.243E-13	2.473E-04	1.114E-05
B0	Coefficient	9.863E-01	1.005E+00	1.135E+00	9.708E-01	9.391E-01	1.000E+00
	C .L.	2.737E-02	4.298E-02	1.828E-01	2.016E-01	1.473E-01	1.076E-01
	P-value	2.779E-09	2.416E-08	1.75644E-05	2.129E-07	5.990E-05	1.340E-05
B1	Coefficient	1.821E-02	1.984E-02	2.610E-02	1.539E-01	2.222E-02	2.734E-02
	C .L.	5.570E-04	8.748E-04	3.719E-03	1.584E-02	8.551E-03	6.247E-03
	P-value	4.518E-09	2.812E-08	9.61193E-06	7.194E-11	1.957E-03	2.633E-04
B2	Coefficient				-9.248E-04	-1.061E-04	-7.489E-05
	C .L.				1.801E-04	9.199E-05	6.720E-05
	P-value				1.053E-07	3.279E-02	3.643E-02

References

- Al-Sabagh A.M., Abdul-Raouf M.E., Abdel-Raheem R., Surface activity and light scattering investigation for some novel aromatic polyester amine surfactants, *Colloids and Surfaces A: Physicochem. Eng. Aspects*, 251, (2004) 167-174. <http://dx.doi.org/10.1016/j.colsurfa.2004.07.012>
- Antonarakis S., Androulaki E., Dimotikali D., Hiskia A., Papaconstantinou E., *Photolytic degradation of all chlorophenols with polyoxometallates and H₂O₂*, *J. Photochemistry and Photobiology A: Chemistry*, 148, (2002) 191-197. [http://dx.doi.org/10.1016/S1010-6030\(02\)00042-4](http://dx.doi.org/10.1016/S1010-6030(02)00042-4)
- Barzetti T., Selli E., Moscotti D., Forni L., Pyridine and ammonia as probes for FTIR analysis of solid acid catalysts, *J. Chem. Soc., Faraday Trans. 92* (1996) 1401-1407. [DOI: 10.1039/FT9969201401](https://doi.org/10.1039/FT9969201401)
- Bhattacharyya A. , Kawi S., Ray M. B., *Photocatalytic degradation of orange II by TiO₂ catalysts supported on adsorbents*, *Catal. Today*, 98, 431-439 (2004). [DOI:10.1080/09593330.2010.495399](https://doi.org/10.1080/09593330.2010.495399)
- Brinker C. J., Scherer G.W., *Sol-gel Science, The Physics and Chemistry of Sol-gel Processing*, Academic press, San Diego, 1990.
- Christophe J.B., Francine A., Pascal C., Marie J., Frank L., *Nanocrystalline Titanium Oxide Electrodes for Photovoltaic Applications*, *J. Am. Ceram. Soc.* 80 (1997) 3157-3171. [DOI: 10.1111/j.1151-2916.1997.tb03245.x](https://doi.org/10.1111/j.1151-2916.1997.tb03245.x)
- Chun H., Yuchao T., Hangxio T., *Characterization and photocatalytic activity of transition-metal-supported surface bond-conjugated TiO₂/SiO₂*, *Catal. Today* 90 (2004) 325-330. <http://dx.doi.org/10.1016/j.cattod.2004.04.042>
- Dalia E. Mohamed, Mohamed A. Abbas, Nesserin A.Fathalla, Marwa R. Mishrif, *Surface activity and light scattering investigation for some novel aromatic polyester amine surfactants*, *Materials Science*, 10(2), 57-71. [DOI: 10.1021/ja00053a020](https://doi.org/10.1021/ja00053a020)
- De Witte K., Busuioc A.M., Meynen V., Mertens M., Bilba N., Van Tendelo G., Cool P., Vansant E.F., *Influence of the synthesis parameters of TiO₂-SBA-15 materials on the adsorption and photodegradation of rhodamine-6G*, *Microporous Mesoporous Mater.* 110 (2008) 100-110. [DOI: 10.1002/adfm.200700783](https://doi.org/10.1002/adfm.200700783)
- Ding Z., Lu G. Q., Greenfield P. F., *Role of the Crystallite Phase of TiO₂ in Heterogeneous Photocatalysis for Phenol Oxidation in Water*, *J. Phys. Chem. B* 104 (2000) 4815-4820. [DOI: 10.1002/anie.200704788](https://doi.org/10.1002/anie.200704788)

Duran A., Serna C., Fornes V., Fernandez-Navarro J.M., Structural considerations about SiO₂ glasses prepared by sol-gel, J. Non-Cryst. Solids 82 (1986) 69-77.
[http://dx.doi.org/10.1016/0022-3093\(86\)90112-2](http://dx.doi.org/10.1016/0022-3093(86)90112-2)

Dutoit D.C.M., Schmeider M., Baiker A., Titania-Silica Mixed Oxides: I. Influence of Sol-Gel and Drying Conditions on Structural Properties, J. Catal. 153 (1995) 165-176. [http://dx.doi.org/10.1016/0926-860X\(95\)00048-8](http://dx.doi.org/10.1016/0926-860X(95)00048-8)

Fujishima A., Rao N.T., Rryk D.A., Titanium dioxide photocatalysis, J. Photochem. Photobiol. C: Rev. 1 (2000) 1-21. [http://dx.doi.org/10.1016/S1010-6030\(03\)00428-3](http://dx.doi.org/10.1016/S1010-6030(03)00428-3)

Hanafi S.A., Gobara H.M., Elmelawy M.S., Abo-El-Enein S.A. and Alkahlawy A.A., Catalytic performance of dealuminated H-Y zeolite supported bimetallic nanocatalysts in Hydroisomerization of n-hexane and n-heptane, Egyptian J. of Petrol. (EJYP), 23(2) (2014). <http://dx.doi.org/10.1016/j.ejpe.2014.02.015>

He C., Tian B., Zhang J., Thermally stable SiO₂-doped mesoporous anatase TiO₂ with large surface area and excellent photocatalytic activity, J. Colloid Interface Sci. 344 (2010) 382-389.
<http://dx.doi.org/10.1016/j.jcis.2010.01.002>

Herrmann J.-M., Heterogeneous photocatalysis: state of the art and present applications In honor of Pr. R.L. Burwell Jr. (1912–2003), Former Head of Ipatieff Laboratories, Northwestern University, Evanston (Ill). Topics in Catalysis, 34 (2005) 49-65. DOI: 10.1017/s11244-005-3788-2

Hoffmann J.P., 2010. Linear Regression Analysis: Applications and Assumptions. Second Edition, Brigham Young, University, Provo.
[https://sociology.byu.edu/Hoffmann/SiteAssets/Hoffmann%20 %20Linear%20Regression%20Analysis %20second%20edition.pdf](https://sociology.byu.edu/Hoffmann/SiteAssets/Hoffmann%20%20Linear%20Regression%20Analysis%20second%20edition.pdf)

Hreczuch W., Trathnig B.; Dziwinski E. and Pyzalsk K.i, Direct Ethoxylation of a Longer-Chain Aliphatic Ester, J. Surfact. Deterg., 4 (2001)167-175. DOI: [10.1007/s11743-001-0171-7](https://doi.org/10.1007/s11743-001-0171-7)

Hu C., Wang Y., Tang H., Influence of adsorption on the photodegradation of various dyes using surface bond-conjugated TiO₂/SiO₂ photocatalyst, Appl. Catal., B 35 (2001) 95-105. [http://dx.doi.org/10.1016/S0926-3373\(01\)00236-3](http://dx.doi.org/10.1016/S0926-3373(01)00236-3)

Hu`sing N., Launay B., Doshi D., Kickelbick G., Mesostructured Silica-Titania Mixed Oxide Thin Films, Chem. Mater. 14 (2002) 2429- 2432. DOI: [10.1021/cm011310z](https://doi.org/10.1021/cm011310z)

Ilyas H., Qazi I. A., Asgar W., Awan M. A., and Khan Z., Photocatalytic Degradation of Nitro and Chlorophenols Using Doped and Undoped Titanium Dioxide Nanoparticles, J. Nanomaterials, 2011 (2011) **Article ID 589185, doi:10.1155/2011/589185**

Kang M., Suk-Jin C., Park J. Y., Photocatalytic performance of nanometer-sized Fe_xO_y/TiO₂ particle synthesized by hydrothermal method, Catal. Today, 87 (2003) 87-97. <http://dx.doi.org/10.1016/j.cattod.2003.09.011>

Katsunori K., Puyam S.S., Titanium-Containing Porous Silica Prepared by a Modified Sol-Gel Method, J. Phys. Chem. B 103 (1999) 3563-3569. [http://dx.doi.org/10.1016/S1387-1811\(00\)00193-1](http://dx.doi.org/10.1016/S1387-1811(00)00193-1)

Kim W.I., Hong I.K., Synthesis of Monolithic Titania-Silica Composite Aerogels with Supercritical Drying Process, J. Ind. Eng. Chem. 9 (6) (2003) 728-734. <http://dx.doi.org/10.1016/j.apcatb.2006.07.022>

Lee M.S., Lee G.D., Hong S.S., J. Ind. Eng. Chem. 9 (5) (2003) 556.
<http://dx.doi.org/10.1016/j.colsurfa.2004.10.014>

Linsebigler A., Lu G., Yates J.T., Photocatalysis on TiO₂ Surfaces: Principles, Mechanisms, and Selected Results, Chem. Rev. 95 (1995) 735-758. DOI: [10.1021/cr00035a013](https://doi.org/10.1021/cr00035a013)

Lippens B.C., Linsen B.G., de Boer J.H., Studies on pore systems in catalysts I. The adsorption of nitrogen; apparatus and calculation, *J. Catal.* 3 (1964) 32-37. [http://dx.doi.org/10.1016/0021-9517\(64\)90089-2](http://dx.doi.org/10.1016/0021-9517(64)90089-2)

Mikhail R. Sh., Brunaer S., Bodor E.E., Investigations of a complete pore structure analysis: I. Analysis of micropores, *J. Colloid Interface Sci.* 26 (1968) 45-53. [http://dx.doi.org/10.1016/0021-9797\(68\)90270-1](http://dx.doi.org/10.1016/0021-9797(68)90270-1)

Pan J.H., Zhao X.S., Lee W.I., Block copolymer-templated synthesis of highly organized mesoporous TiO₂-based films and their photoelectrochemical applications, *Chem. Eng. J.* 170 (2011) 363-380. <http://dx.doi.org/10.1016/j.cej.2010.11.040>

Radwa A. Elsalamony, Ph.D. Thesis, "Photocatalytic degradation of organic pollutants containing various functionalities in aqueous solution using transition metal oxides as photocatalysts" Faculty of Science Ein Shams University, Cairo, Egypt (2010).

Rubio J., Oteo J.L., Villegas M., Duran P., Characterization and sintering behaviour of submicrometre titanium dioxide spherical particles obtained by gas-phase hydrolysis of titanium tetrabutoxide, *J. Mater. Sci.* 32 (1997) 643-652. **DOI:10.1023/A:1018579500691**

Sayilkan F., Asilturk M., Sener S., Erdemoglu S., Erdemoglu M., Sayilkan H., Hydrothermal Synthesis, Characterization and Photocatalytic Activity of Nanosized TiO₂ Based Catalysts for Rhodamine B Degradation, *Turk. J. Chem.* 31 (2007) 211-221.

Schraml-Marth M., Walther K.L., Wokaun A., Handy B.E., Baiker A., Porous silica gels and TiO₂/SiO₂ mixed oxides prepared via the sol-gel process: characterization by spectroscopic techniques, *J. Non-Cryst. Solids* 143 (1992) 93-111. [http://dx.doi.org/10.1016/S0022-3093\(05\)80557-5](http://dx.doi.org/10.1016/S0022-3093(05)80557-5)

Sheu, E. Y. and Mullins, O. C., *Asphaltenes: Fundamentals and Applications*, Plenum Press, New York, 1995.

Shiraishi Y., Saito N., Hirai T., Adsorption-Driven Photocatalytic Activity of Mesoporous Titanium Dioxide, *JACS* 127 (2005) 12820-12822. DOI: 10.1021/ja053265s

Sing K. S. W., Everett D. H., Haul R. A. W., Moscou, L., Pierotti, R. A., Reporting physisorption data for gas/solid systems with special reference to the determination of surface area and porosity, *Pure and Applied Chemistry*, 57 (1985) 603-619.
Sons Inc., New Jersey. Present

Tanaka K., Padermpole K., Hisaagam T., Photocatalytic degradation of commercial azo dyes, *Water Res.* 34 (2000) 327-333. [http://dx.doi.org/10.1016/S0043-1354\(99\)00093-7](http://dx.doi.org/10.1016/S0043-1354(99)00093-7)

Tanev P.T., Chibwe M., Pinnavaia T.J., Titanium-containing mesoporous molecular sieves for catalytic oxidation of aromatic compounds, *Nature* 368 (1994) 321-323. [doi:10.1038/378159a0](https://doi.org/10.1038/378159a0)

Viswanath R.N., Bose A.C., Ramasamy S., Preparations and characterizations of nanostructured TiO₂ and TiO₂-Si(Ti)O₂ composite systems, *J. Phys. Chem. Solids* 62 (2001) 1991-1998. <http://eprints.qut.edu.au>

Walker J.V., Morey M., Carlsson H., Davidson A., Stucky G.D., Butler A.J., Peroxidative Halogenation Catalyzed by Transition-Metal-Ion-Grafted Mesoporous Silicate Materials, *J. Am. Chem. Soc.* 119 (1997) 6921-6922. **DOI: 10.1021/ja971063t**

Weisberg S., 2005. *Applied Regression Analysis*, third Edition, John Wiley and
Yu J.C., Yu J., Zhao J., Enhanced photocatalytic activity of mesoporous and ordinary TiO₂ thin films by sulfuric acid treatment, *Appl. Catal. B: Environ.* 36 (2002) 31-43. [http://dx.doi.org/10.1016/S0926-3373\(01\)00277-6](http://dx.doi.org/10.1016/S0926-3373(01)00277-6)

Zhu Y., Zhang L., Yao W., Cao L., The chemical states and properties of doped TiO₂ film photocatalyst prepared using the Sol-Gel method with TiCl₄ as a precursor, *Appl. Surf. Sci.* 158 (2000) 32-37.

The IISTE is a pioneer in the Open-Access hosting service and academic event management. The aim of the firm is Accelerating Global Knowledge Sharing.

More information about the firm can be found on the homepage:
<http://www.iiste.org>

CALL FOR JOURNAL PAPERS

There are more than 30 peer-reviewed academic journals hosted under the hosting platform.

Prospective authors of journals can find the submission instruction on the following page: <http://www.iiste.org/journals/> All the journals articles are available online to the readers all over the world without financial, legal, or technical barriers other than those inseparable from gaining access to the internet itself. Paper version of the journals is also available upon request of readers and authors.

MORE RESOURCES

Book publication information: <http://www.iiste.org/book/>

IISTE Knowledge Sharing Partners

EBSCO, Index Copernicus, Ulrich's Periodicals Directory, JournalTOCS, PKP Open Archives Harvester, Bielefeld Academic Search Engine, Elektronische Zeitschriftenbibliothek EZB, Open J-Gate, OCLC WorldCat, Universe Digital Library, NewJour, Google Scholar

